

MINIMUM USAGE OF FERRITE TILES IN ANECHOIC CHAMBERS

S. M. J. Razavi, M. Khalaj-Amirhosseini, and A. Cheldavi

College of Electrical Engineering
Iran University of Science and Technology
Tehran, Iran

Abstract—Anechoic chambers which are used for emission and immunity testing require expensive ferrite tiles on their inner surfaces. This paper describes a method to reduce the number of required ferrite tiles, whilst ensuring a reliable and specified test region. In this method, the positions of some ferrite tiles are found optimally to keep the performance of the anechoic chamber as high as possible. An optimum ray-tracing method is presented to predict the electric field in the anechoic chamber. The performance of the proposed method is verified by a comprehensive example simulated by the CST software, which is a full-wave simulator based on time difference method.

1. INTRODUCTION

The need for indoor testing of electromagnetic radiating devices, which began in the early 1950s [1], has led to a number of companies providing chambers and absorber products supporting a range of electromagnetic testing requirements. Microwave anechoic chambers are currently in use for a variety of indoor antenna measurements, electromagnetic interference (EMI) measurements, and electromagnetic compatibility (EMC) measurements. The anechoic chamber provides a test volume, called the “quiet zone”, in which the level of reflected waves determines the performance of the anechoic chamber.

Some series of materials have been developed for absorption in the 30 to 1000 MHz frequency range. The most common material is ferrite tile. Ferrite tiles are expensive, and the room strength required to support the weight of the tiles (of the order of 30 kg/m²) adds to the cost. The need for decreasing the cost led to the development of some optimized analytical and practical methods. Based on experiments [2],

Corresponding author: S. M. J. Razavi (razavismj@yahoo.com).

with 80% of the Fresnel zone [3] covered for absorption the variation of the E -field is very uniform at all frequencies above 300 MHz, and the maximum error is approximately 1.4 dB. It is possible to cover just 80% of the surface of the chamber with ferrite absorber and obtain a response which is within ± 4 dB of the free space response between 40 and 200 MHz [4]. Some other optimization methods using additional absorbers, shifted absorbers, and optimized absorbers are proposed in [5].

In this paper, a new method is proposed to reduce the need for full coverage using ferrite tiles and to optimize the layout of ferrite tiles to reach good performance and minimize cost. The proposed method has been simulated via computer programs and is validated with the CST software.

The modeling technique is described in Section 2. Section 3 presents an example and the results of the work. Conclusions are given in Section 4.

2. MODELING TECHNIQUE

In the first step, the electric field in the anechoic chamber is evaluated for a dipole antenna using the optimum ray-tracing method, described in Section 2.1. The next step explains the proposed algorithm, described in Section 2.2, to determine the layout of ferrite tiles in the inner surfaces of the chamber to produce the best performance. The model of a ferrite tile over a wide frequency range is described in Section 2.3.

2.1. Optimum Ray-tracing Method

The known ray tracing technique which is based on geometrical optics (GO) provides a relatively simple solution for indoor wave propagation. It should be noted that using the GO and ray tracing technique is valid only when the object of interest has dimensions greater than the wavelength.

In the ray tracing method, the waves radiated from a transmitting antenna can be modeled as many ray tubes shooting from the location of the antenna [6, 7]. In a ray-tracing program, each ray tube may be composed of four rays separated by the increments of θ and φ ($\Delta\theta$ and $\Delta\varphi$) in local spherical coordinates, centered at the antenna. To generate the ray tubes, a sphere of radius r centered at the antenna is divided into quadrilateral cells that are close to squares with approximately the same area by selecting a fixed $\Delta\theta$ and a

$\Delta\varphi = \Delta\theta / \sin\theta$. Fig. 1 shows the simulated region that is an anechoic chamber with six boundary surfaces.

In the conventional ray-tracing procedure, the rays have been traced one by one [6–8, 14, 15], taking a large run time. To speed up the ray tracing algorithm, we propose to trace the rays simultaneously. In this way, the ray-tracing procedure may be modified by the following two steps:

- 1) The boundary surfaces intersected with all rays have to be found at one time. Consider one of the boundary surfaces with a rectangular shape as shown in Fig. 2 whose normal unit vector is \hat{n}_i . One plane (oa_ja_{j+1}), in which $j = 1, 2, 3, 4$, o is the point source and a_j s are the edge points of the boundary surface, is passed through each side of this boundary surface ($\overline{a_ja_{j+1}}$) and the point source. The normal unit vector of each defined plane can be determined from the following expression:

$$\hat{n}_{ij} = \frac{\overrightarrow{oa_j} \times \overrightarrow{oa_{j+1}}}{|\overrightarrow{oa_j} \times \overrightarrow{oa_{j+1}}|} \tag{1}$$

In (1), if $j + 1$ becomes greater than 4, it is replaced by 1.

A function f is defined such that it takes 1 for the rays incident to the boundary surface No. i and takes zero for the other rays.

$$f(i, \hat{r}) = 1 + \text{sign} \left(\sum_{j=1}^4 \text{sign}(\hat{n}_{ij} \cdot \hat{r}) - 4 \right) \tag{2}$$

where \hat{r} is directional vector of the incident ray and sign is the sign function.

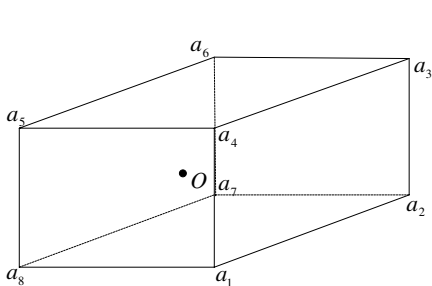


Figure 1. Geometry of an anechoic chamber.

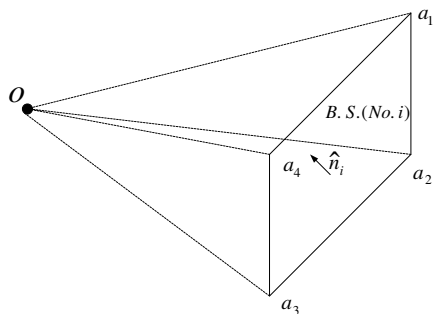


Figure 2. Boundary surface number i ; $i = 1, 2, 3, 4, 5, 6$ and source point.

- 2) The sum of the products of defined functions f and the normal unit vectors \hat{n}_i give us the normal unit vector of the corresponding boundary surfaces of all rays, at one time, as the following relation:

$$\hat{n} = \sum_{i=1}^6 f(i, \hat{r}) \cdot \hat{n}_i \quad (3)$$

Also, an arbitrary point of corresponding boundary surfaces of all rays can be found using a similar expression as follows:

$$P = \sum_{i=1}^6 f(i, \hat{r}) \cdot P_i \quad (4)$$

where P_i is an arbitrary point on the intersecting boundary surfaces No. i .

The other steps are similar to the known ray-tracing algorithm proposed in [8]. It is worth mentioning that the proposed ray tracing algorithm could be useful in numerical software, such as MATLAB which based on matrix operations.

To calculate the reflection field at each point P_i on the boundary surfaces No. i , as shown in Fig. 3, use following relation.

$$\vec{E}_r = \left\{ \left[\Gamma_{TE} \left(\hat{u}_{TE} \cdot \vec{E}_t \right) \right] \hat{u}'_{TE} + \left[\Gamma_{TM} \left(\hat{u}_{TM} \cdot \vec{E}_t \right) \right] \hat{u}'_{TM} \right\} \quad (5)$$

where Γ_{TE} and Γ_{TM} are the complex reflection coefficients for the waves polarized perpendicular and parallel to the plane of incidence respectively [9].

\hat{u}_{TE} is the unit vector perpendicular to the incident plane and given by

$$\hat{u}_{TE} = \frac{(\hat{r} \times \vec{n}_i)}{|\hat{r} \times \vec{n}_i|} \quad (6)$$

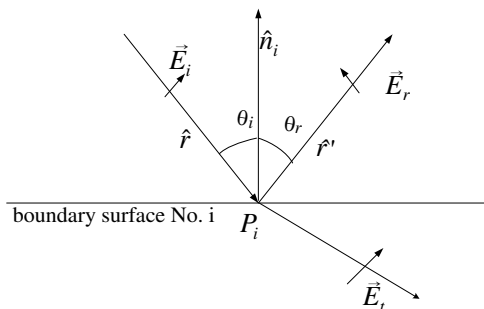


Figure 3. The reflected and transmitted rays in the plane of incidence.

where \hat{r} is unit vector along incident ray and the reflected ray along \hat{r}' also lies in the same incident plane, i.e.,

$$\hat{u}'_{TE} = \hat{u}_{TE} \tag{7}$$

\hat{u}_{TM} is a unit vector parallel to the plane of incidence and also perpendicular to the direction

$$\vec{u}_{TM} = \frac{(\hat{r} \times \hat{u}_{TE})}{|\hat{r} \times \hat{u}_{TE}|} \tag{8}$$

For the reflected ray the corresponding unit vector is given as

$$\hat{u}'_{TM} = -\frac{(\hat{r}' \times \hat{u}_{TE})}{|\hat{r}' \times \hat{u}_{TE}|} \tag{9}$$

2.2. Optimized Algorithm for Setting Absorber Material

The aim of this work is to reduce the amount of ferrite tiles and find their positions optimally to produce “best” performance for the

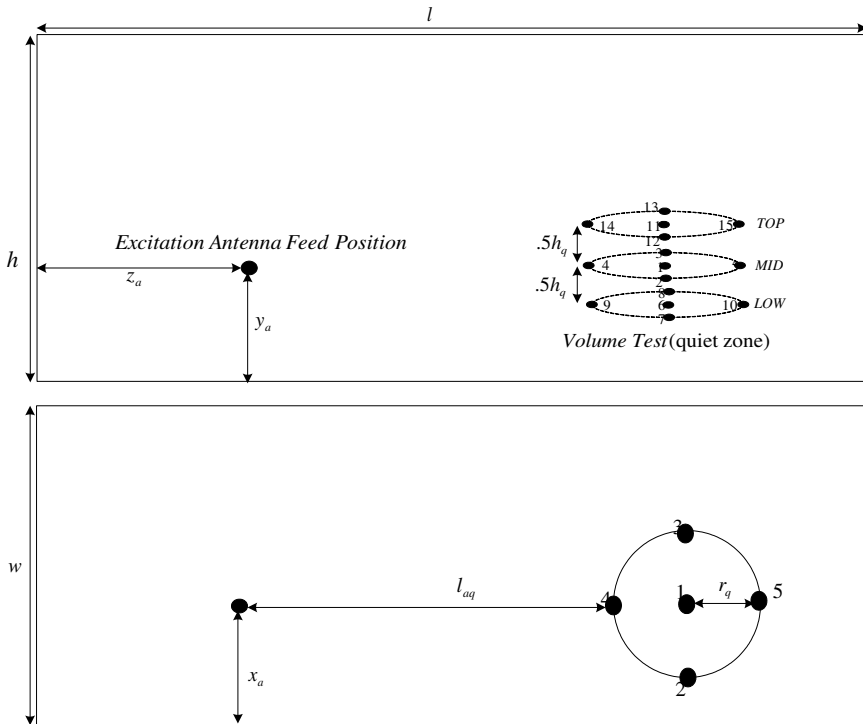


Figure 4. Positions of excitation antenna feed and 15 test point volume.

anechoic chamber. For this purpose, 15 points of the quiet zone were selected as the test points. Fig. 4 shows the top-view and side-view of the anechoic chamber along with the positions of the feed of excitation antenna and the test points.

The proposed optimization algorithm is based on the following five steps:

- 1) The inner surface of the chamber is meshed by using a rectangular grid with square cells of the size $\Delta l \times \Delta l$, where Δl represents the resolution factor of the analysis method.
- 2) A cost matrix with initial zero value is defined and assigned for this grid, so that each element of the matrix corresponds to the one cell of the grid.
- 3) In each iteration, the cells that ray tubes strike before passing from the test points are found. An instantaneous cost matrix with the value of one for these cells and zero for the other cells is defined.
- 4) The defined cost matrix is updated by the following equation in the i th iteration:

$$\text{cost_matrix}(i) = \text{cost_matrix}(i-1) + (\text{inst_cost_matrix}(i)/i) \quad (10)$$

- 5) The optimization process will be terminated if the magnitude of the all E -fields is less than a threshold.

At the end of the optimization process, the cost matrix is obtained so that the important cells have higher values than the other ones. To reduce the need for full coverage using ferrite tiles and to minimize the cost, the cells with low values in the cost matrix are not covered with ferrite tiles. It is done considering the desired coverage percent of ferrite tiles. The above discussion has been quantified in the results section.

The proposed optimization algorithm is simple and about 24 times faster than the conventional methods such as a genetic algorithm [8]; for example in a special case the run of the proposed method took about 30 minutes on a normal PC while it took more than 12 hours for the genetic algorithm.

2.3. Representing Ferrite Tiles

Ferrite tiles are made of solid ferrite of about 6 mm thickness or in a grid construction of approximately 20 mm thickness. The frequency response of these ferrite tiles cannot be modeled accurately over a wide frequency range [16]. This is due to the change in their permeability with frequency. To consider frequency-dependent material behavior in broadband simulations, the most common models up to second-order

dispersions are available [10, 11]. These models include relaxation and resonance effects as well as plasma or even gyrotropic media.

The relaxation process, also called *first-order Debye model* is characterized by the following formulation for the relative permeability, containing the relaxation time τ , infinity permeability μ_∞ and static permeability μ_s [10, 11].

$$\mu(\omega) = \mu_\infty + \frac{\mu_s - \mu_\infty}{1 + j\omega\tau} \tag{11}$$

Figure 5 shows the real and imaginary parts of the relative permeability of one of the commercial ferrite tile absorbers and their simulation models. For this type of ferrite $\tau = 33.22$ ns, $\mu_\infty = \mu_0$ and $\mu_s = 1394.5\mu_0$ where μ_0 is the vacuum permeability. The relative permittivity of this compound is approximately equal to 11.

When a ray tube is incident on the ferrite tile, a reflected and a transmitted ray tube is generated according to Snell's law and the local plane wave approximation. The reflection and transmission coefficients of the TE and TM plane wave illuminating a flat interface of two materials are employed in all text books such as [9]. In the electromagnetic anechoic chamber, the back of ferrite tiles is a perfect electric conductor, which has been considered in simulation.

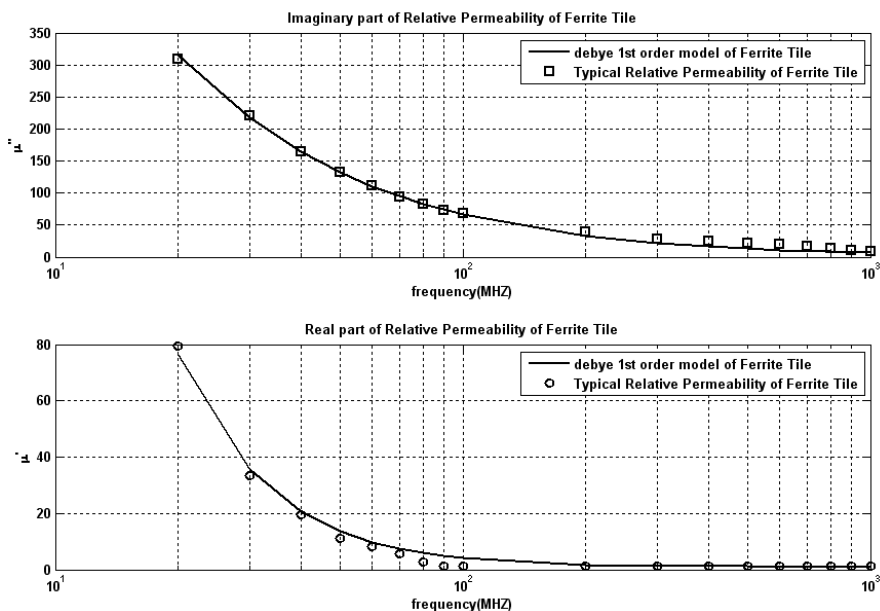


Figure 5. Relative permeability of a ferrite tile.

3. RESULTS

The proposed method is applied to optimize a practical anechoic chamber such as EMC test chamber compact TC800-20 [12].

The characteristics of this chamber are listed in Table 1. The excitation antenna feed position is $(x_a, y_a, z_a) = (1.5, 1, 2)$ m and the other parameters shown in Fig. 4 are $h_q = 1$ m, $r_q = .75$ m and $l_{aq} = 2.25$ m. As previously explained in Section 2.2, the elements of the cost matrix are assigned high values for the important cells and low values for the non important cells, and then the ferrite tiles are used only in the important cells of the inner surface of the anechoic chamber. For this purpose the high value elements of the cost matrix have been specified by a suitable threshold level. For testing and validating the layout of ferrite tiles, the field uniformity of anechoic chamber has been calculated by CST software.

The most often quoted procedure is to require the field in the test region of the chamber to be uniform within 0 to 6 dB over 75 percent of the test points within an aperture centered in the test region [13]. The aperture, as shown in Fig. 6, is defined to be 1 m \times 1.5 m, starting at a height of .5 m above the ground plane and is discretized by 12 points. Therefore, the fields of at least nine of these twelve points have to be within the 0 to 6 dB requirement, where all E -fields are normalized to the lowest E -field level.

Table 1. The characteristics of EMC test chamber compact TC800-20.

Dimensions $l \times w \times h$	Frequency range:	Measuring distance:	Quite zone:
7 m \times 3 m \times 3 m	26 MHz to 1 GHz	Up to 3.0 m	1.5 m dia. Cylinder @ 1 m height

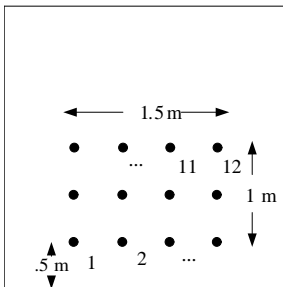


Figure 6. Arrangement of test points specified in the uniform field test procedure.

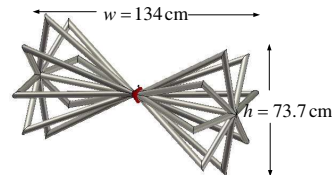


Figure 7. The geometric of biconical antenna.

The results of this work are explained in the following subsections.

3.1. Excitation Antenna

For the field uniformity tests at low frequencies, usually biconical antennas are used. The dimensions of the used biconical antenna are shown in Fig. 7. Also, the simulation results of this antenna are shown in Figs. 8 and 9.

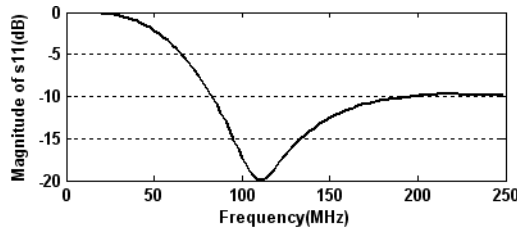


Figure 8. Parameter S_{11} of the biconical antenna over a wide range of frequencies.

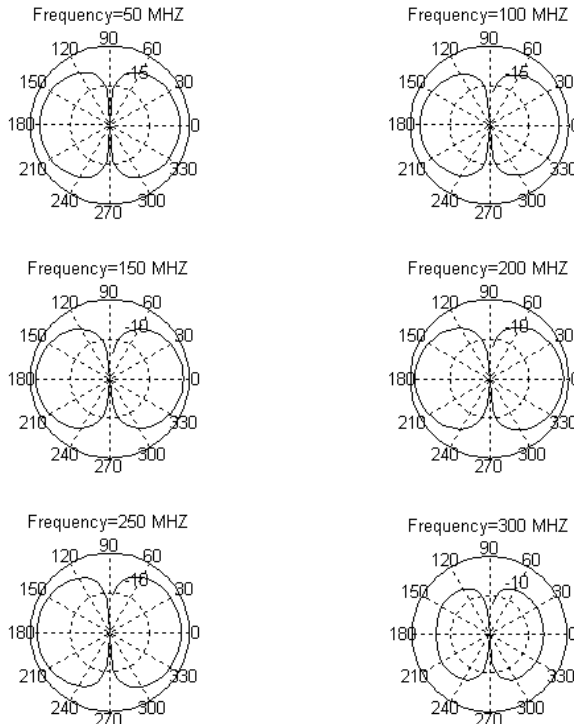


Figure 9. Wide band pattern of the biconical antenna.

3.2. 90% and 85% Coverage of Ferrite Tiles

The inner surface of the anechoic chamber is meshed by using a rectangular grid with square cells of the size 20 cm. In the first example, 90% of the inner surface of the anechoic chamber which has a high value in the cost matrix is covered by ferrite tiles. The obtained layout of ferrite tiles is shown in Fig. 10. Nearly all of the cells of the back and front walls are found to be important and therefore have to be covered by ferrite tiles.

Figure 11 shows the parameter S_{11} of the excitation antenna, which is acceptable compared with Fig. 8. Also, the relative levels of the E -fields are within an acceptable range (0 to 6 dB) for most of the twelve test points as shown in Fig. 12.

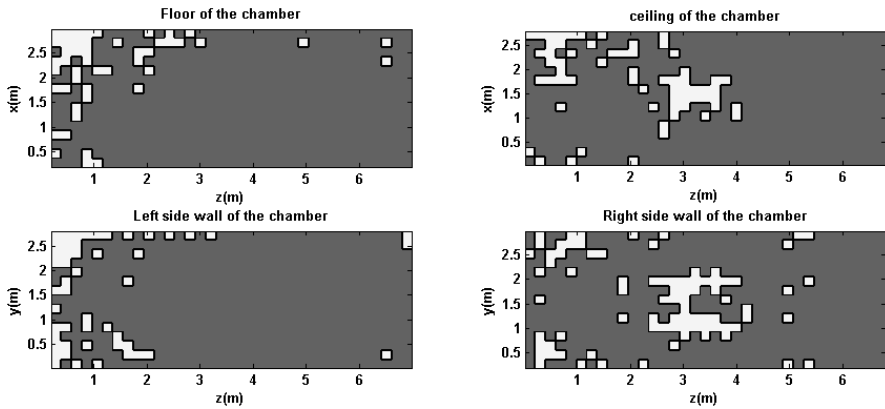


Figure 10. Optimized layout of ferrite tiles for 90% coverage of the inner surface of the anechoic chamber (black=tiles, white=no tiles).

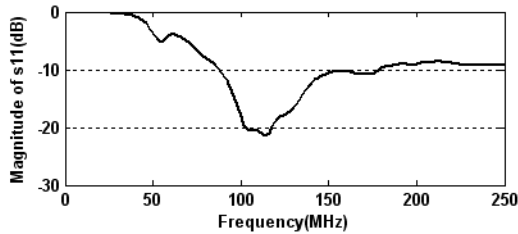


Figure 11. Parameter S_{11} of the excitation antenna in the anechoic chamber with 90% coverage of ferrite tiles.

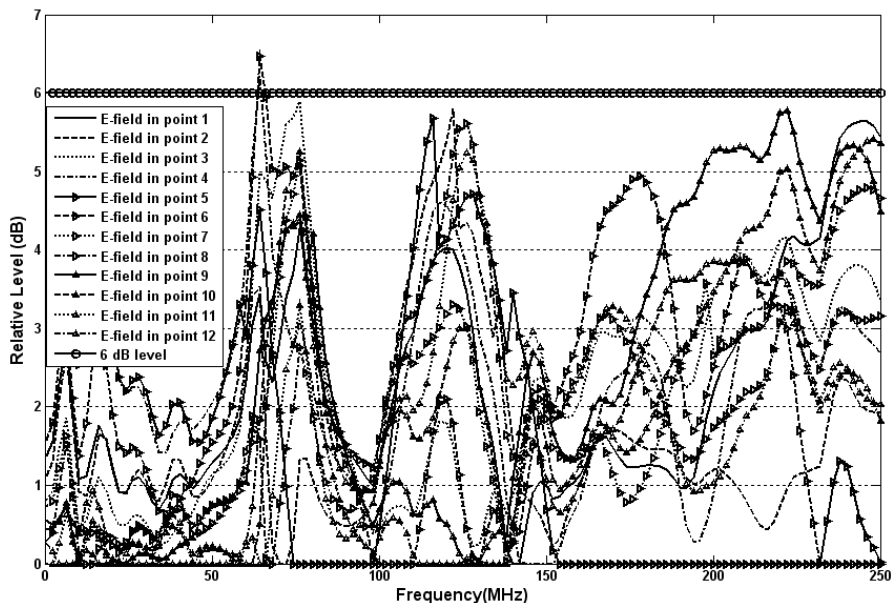


Figure 12. Field uniformity test result in the anechoic chamber with with 90% coverage of ferrite tiles.

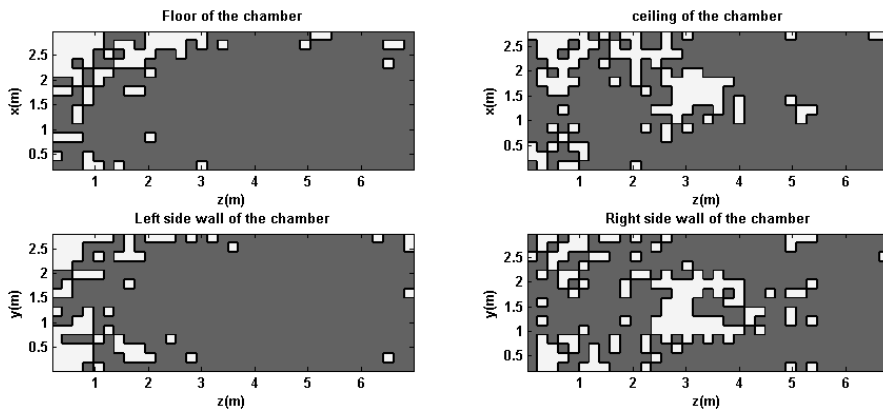


Figure 13. Optimized layout of ferrite tiles for 85% coverage of the inner surface of the anechoic chamber (black=tiles, white=no tiles).

In the second example, 85% of the inner surface of the anechoic chamber which has a high value in the cost matrix is covered by ferrite tiles. The obtained results of this example are shown in Figs. 13, 14, and 15. Again, it is seen that the results are acceptable.

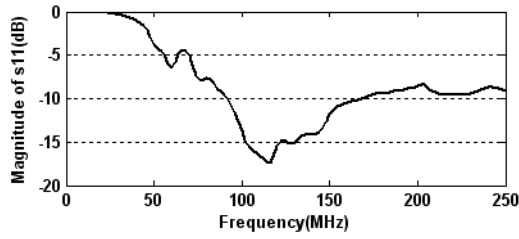


Figure 14. Parameter S_{11} of the excitation antenna in the anechoic chamber with 85% coverage of ferrite tiles.

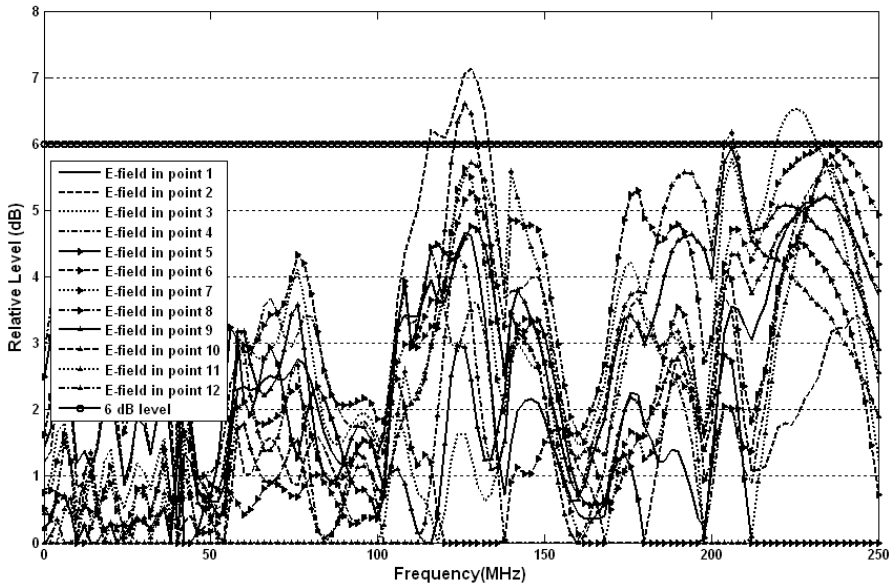


Figure 15. Field uniformity test results in the anechoic chamber with 85% coverage of ferrite tiles.

3.3. 80% Coverage of Ferrite Tiles

In the third example, 80% of the inner surface of anechoic chamber which has a high value in the cost matrix is covered by ferrite tiles. The obtained results of this example are shown in Figs. 16, 17, and 18. It is seen that the results are not acceptable, because the field uniformity and the parameter S_{11} of the excitation antenna are poor. Now, one may be conclude that the optimum coverage of ferrite tiles is between 80–85% of the inner surface of the anechoic chamber.

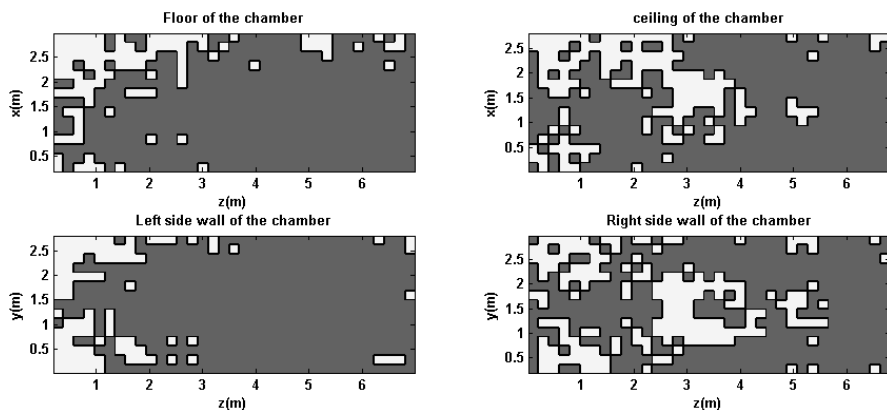


Figure 16. Optimized layout of ferrite tiles for 80% coverage of the inner surface of the anechoic chamber (black=tiles, white=no tiles).

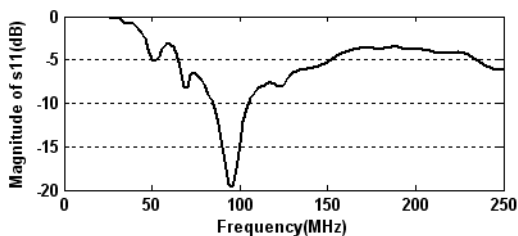


Figure 17. Parameter S_{11} of the excitation antenna in the anechoic chamber with 80% coverage of ferrite tiles.

3.4. 83% Coverage of Ferrite Tiles

In the fourth example, a trial-and-error search has been applied to find optimum coverage of ferrite tiles within the allowable range. The optimum coverage of ferrite tiles was obtained for 83% of the inner surface of the anechoic chamber. The results of this optimum layout are shown in Figs. 19, 20, and 21. It is seen that the results are acceptable. Therefore it is sufficient to cover with ferrite tiles only 83% of the inner surfaces of anechoic chamber having a high value in the cost matrix.

The performance of the anechoic chamber at higher frequencies can be improved by lining loaded carbon foam in the vacant spaces between ferrite tiles.

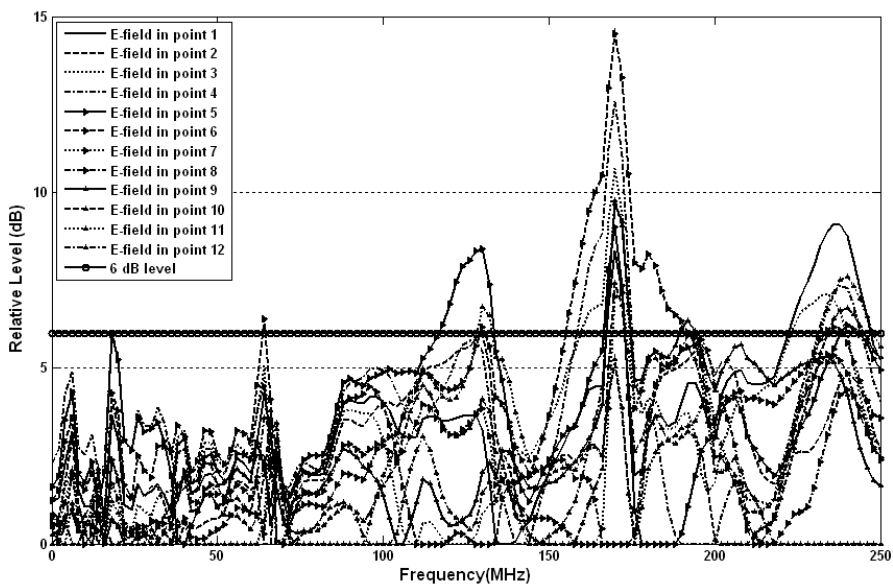


Figure 18. Field uniformity test results in the anechoic chamber with 80% coverage of ferrite tiles.

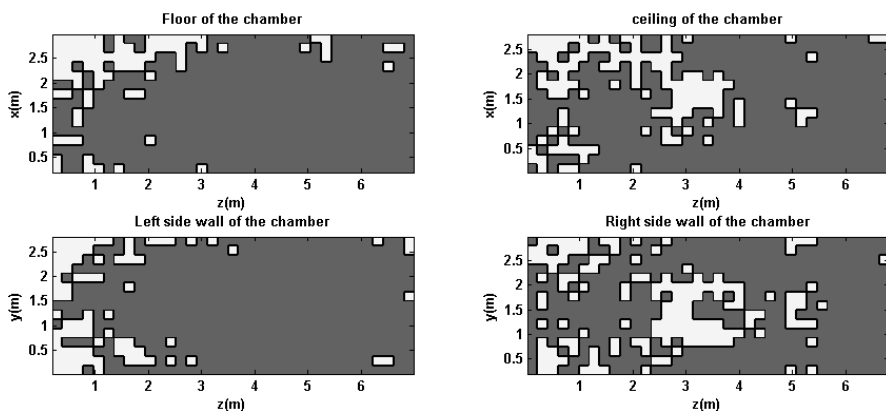


Figure 19. Optimized layout of ferrite tiles for 83% coverage of the inner surface of the anechoic chamber (black=tiles, white=no tiles).

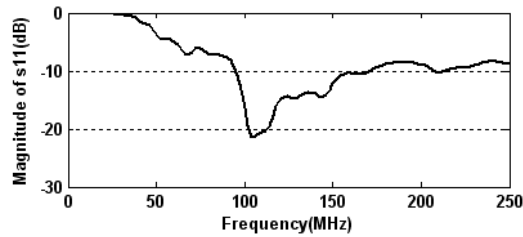


Figure 20. Parameter S_{11} of the excitation antenna in the anechoic chamber with 83% coverage of ferrite tiles.

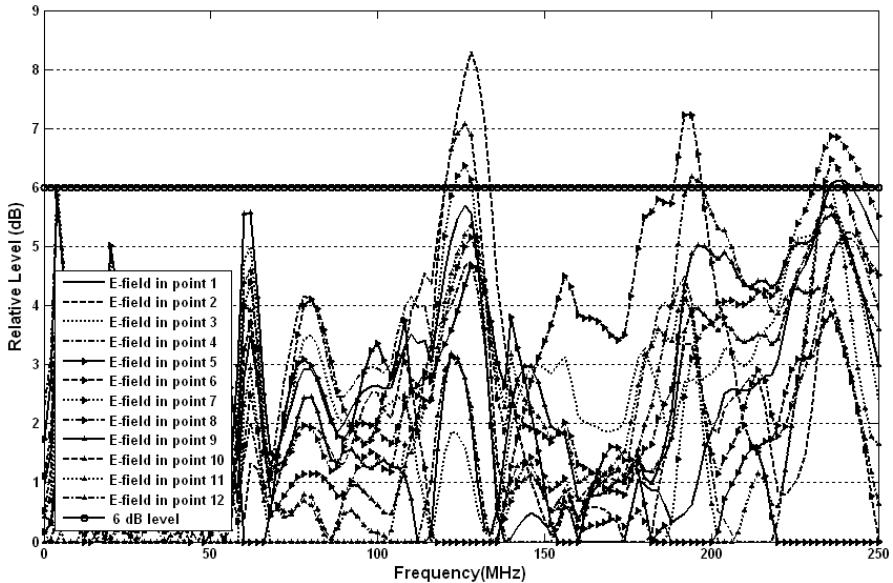


Figure 21. Field uniformity test results in the anechoic chamber with 83% coverage of ferrite tiles.

4. CONCLUSION

In this paper a new method was proposed to optimize an anechoic chamber. The idea of this method is to use a minimum number of ferrite tiles in suitable points of the inner surfaces of the anechoic chamber. The performance of the proposed method was verified by a comprehensive example. The minimum coverage of ferrite tiles and their positions were found optimally to keep the performance of the anechoic chamber as high as possible. After some trial-and-error searching, an anechoic chamber with 83% coverage of ferrite tiles was optimally designed to have acceptable field uniformity over the frequency range of the test.

REFERENCES

1. Emerson, W. H., "Electromagnetic wave absorbers and anechoic chambers through the years," *IEEE Trans. on Ant. and Propag.*, Vol. 21, No. 4, Jul. 1973.
2. Kineros, C. and V. Ungvichian, "A low cost conversion of semi-anechoic chamber to fully anechoic chamber for RF antenna measurements," *IEEE International Symposium on Electromag. Compat.*, Vol. 2, 724–729, Aug. 2003.
3. Collin, R. E., *Antennas and Radio Wave Propagation*, McGraw Hill, 1985.
4. Dawson, L., J. Clegg, S. J. Porter, J. F. Dawson, and M. J. Alexander, "The use of genetic algorithms to maximize the performance of a partially lined screened room," *IEEE Trans. Electromagn. Compat.*, Vol. 44, No. 1, 233–242, Feb. 2002.
5. Bornkessel, C. and W. Wiesbeck, "Numerical analysis and optimization of anechoic chambers for EMC testing," *IEEE Trans. Electromagn. Compat.*, Vol. 38, No. 3, 499–506, Aug. 1996.
6. Yang, C. F., B. C. Wu, and C. J. Ko, "A ray-tracing method for modeling indoor wave propagation and penetration," *IEEE Trans. on Ant. and Propag.*, Vol. 46, No. 6, 907–919, Jun. 1998.
7. Kim, H. and H. Ling, "Electromagnetic scattering from an inhomogeneous object by ray tracing," *IEEE Trans. on Ant. and Propag.*, Vol. 40, 517–525, May 1992.
8. Razavi, S. M. J. and M. Khalaj-Amirhosseini, "Optimization of an anechoic chamber with ray-tracing and genetic algorithms," *Progress In Electromagnetics Research B*, Vol. 9, 53–68, 2008.
9. Balanis, C. A., *Advanced Engineering Electromagnetics*, John Wiley & Sons, 1989.
10. Qi, X., J. Zhou, Z. Yue, Z. Gui, L. Li, and S. Buddhudu, "A ferroelectric ferromagnetic composite material with significant permeability and permittivity," *Advanced Functional Materials*, Vol. 14, No. 9, 920–926, Sept. 2004.
11. Wu, J., M. Y. Koledintseva, and J. L. Drewniak, "FDTD modeling of structures containing dispersive isotropic magnetic materials," *Proc. IEEE Int. Symp. Electromagn. Compat.*, Vol. 2, 904–909, Boston, Aug. 18–22, 2003.
12. www.rfi-ind.com.au/download/Compact%20TC800-20.pdf.
13. CENELEC EN 61000-4-3: 1996, Electromagnetic Compatibility (EMC)-Part 4-3: Testing and Measurement Techniques-Radiated, Radio-Frequency, Electromagnetic Field Immunity Test.

14. Kim, H. and H.-S. Lee, "Accelerated three dimensional ray tracing techniques using ray frustums for wireless propagation models," *Progress In Electromagnetics Research*, PIER 96, 21–36, 2009.
15. Tayebi, A., J. Gómez, F. S. Saez de Adana, and O. Gutierrez, "The application of ray-tracing to mobile localization using the direction of arrival and received signal strength in multipath indoor environments," *Progress In Electromagnetics Research*, PIER 91, 1–15, 2009.
16. Khalaj-Amirhosseini, M. and H. Ghorbaninejad-Foumani, "To compact waveguide devices by dielectric and ferrite layers," *Progress In Electromagnetics Research M*, Vol. 9, 243–255, 2009.